Deoxyribonucleic acid-based electron selective contact for crystalline silicon solar cells

Thomas Tom*[1,2], Eloi Ros*[3], David Rovira[3], Julian López-Vidrier[1,2], José Miguel Asensi[1,2], Pablo Ortega[3], Joaquim Puigdollers[3], Cristobal Voz[3], Joan Bertomeu**[1,2]

[1] Departament de Física Aplicada, Universitat de Barcelona, Barcelona, Spain
[2] Institute of Nanoscience and Nanotechnology (IN2UB), Universitat de Barcelona, Barcelona, Spain
[3] Universitat Politècnica de Catalunya (UPC), 08034 Barcelona, Spain

* Shared co-first authorship
** Corresponding author: jbertomeu@ub.edu

Abstract

Development of carrier selective contacts for crystalline silicon solar cells has been recently of great interest towards the further expansion of silicon photovoltaics. The use of new electron and hole selective layers has opened an array of possibilities due to the low-cost processing and non-doping contacts. Here, a non-doped heterojunction silicon solar cell without the use of any intrinsic amorphous silicon is fabricated using Deoxyribonucleic acid (DNA) as the electron transport layer (ETL) and transition metal oxide V_2O_5 as the hole transport layer. The deposition and characterization of the DNA films on crystalline silicon have been studied, the films have shown a *n*-type behaviour with a work function of 3.42 eV and a contact resistance of 28 mΩ cm^2. This non-doped architecture has demonstrated a power conversion efficiency of 15.6%, which supposes an increase of more than 9% with respect to the cell not containing the biomolecule, thus paving the way for a future role of nucleic acids as ETLs.

Introduction

Deoxyribonucleic acid (DNA) is the most important naturally-driven biomolecule that carries genetic code in all living organisms[1][2]. The structure of DNA was discovered by Watson and Crick half a century ago[3]. DNA-composed layers exhibit unique electrochemical and optical properties with an advantageous biocompatibility and capacity to store information in nucleic acid sequences. DNA has a unique double-helical structure with nucleotide bases linked by hydrogen-bond base pairs connected to a backbone of sugars and phosphates with high-temperature stability of 200–250 °C[4][5]. DNA has been tested as the building block of many optofluidic devices and solid-state devices like organic light emitting diodes (OLEDs) and organic field effect transistors (OFETs)[6][7][8]. Hybrid semiconductor devices implementing DNA might be used in sensors where device functionality responds to the modified optoelectronic properties of the biopolymer. Furthermore, DNA/semiconductor devices might pave the way to electronically interact with complex biological systems, by means of the biocompatible deoxyribonucleic acid interface allowing certain chemical reactions via selective electron/hole conduction.

We turn our attention to crystalline silicon (c-Si), because it is an inexpensive and deeply studied semiconductor that makes for a high-quality substrate in solar energy devices. Use of such a stable and well-documented semiconductor allows an intensive study of the interface with the DNA. Engineering of crystalline silicon solar cells by use of new electron and hole selective layers that do not require substrate doping has opened an array of possibilities for new photovoltaic structures[9][10][11]. Different materials such as metal oxides, nitrides, alkali/alkaline earth metal salts, and organic polymers, have already been proven to work as Electron Transport Layers (ETLs) and Hole Transport Layers (HTLs) on c-Si solar cells. This new research line works to enhance photovoltaic efficiency by eliminating Schottky barriers or Fermi level pinning effects at the interface between the electrode and the semiconductor[12][13][14]. This advantage could be also used in other type of devices that could take advantage of such physicochemical surface properties. Moreover, most of these contacts can be deposited using simple techniques such as thermal evaporation, sputtering, atomic layer deposition (ALD) or spin coating[15][16][17]. Hence, flammable and toxic boron/phosphorous gas precursors used for doping in techniques such as Thermal Diffusion or Plasma-Enhanced Chemical Vapour Deposition (PECVD) can be avoided[18][19].
Recently, the use of DNA has been reported both as electron and hole transport layers in photovoltaic devices[20][21]. Yosoff *et al.* incorporated DNA-hexadecyl trimethyl ammonium chloride (CTMA) as the HTL in solution-processed low-temperature perovskite solar cells, which resulted in a power conversion efficiency (PCE) of 15.86%[22]. In another work, DNA-based hybrid materials were used for interface engineering of polymer solar cells and have achieved an efficiency of 7.6% [23] A recent study by Hou *et al.* demonstrated the extraction and transport of holes in perovskite heterostructure-based solar cells[24]. In their work, instead of incorporating DNA as a separate layer under the perovskite, they used the idea of wrapping the core-shell heterostructure of perovskite by DNA-CTMA through a self-assembling process, which yielded a PCE of 20.63%. The electron transport capacity of DNA has been also studied in recent years by Dajar *et al.* with a reported photovoltaic efficiency of 4.88% in an organic solar cell as the ETL [25]. In another investigation, in which DNA-coated ZnO nanoparticles were used as ETL for polymer solar cells, the authors were able to achieve an efficiency of 8.5%[26]. In addition, Reichel *et al.* have recently demonstrated the usage of DNA nucleobase adenine as an interfacial layer in crystalline silicon (c-Si) heterojunction solar cells[27].

In this work, we report the use of deoxyribonucleic acid-based polymer as the ETL in combination with a c-Si absorber. A thorough study of the optical, electrical, and compositional properties of the used DNA layers, as well as the electronic effect of these layers on the silicon interface, has been carried out. Finally, the material has been successfully implemented in a non-textured dopant-free solar cell to test the performance of the contact in a finished device, obtaining a PCE of 15.6%.

Experimental

Low molecular weight DNA biopolymer was used as the electron selective contact for crystalline silicon solar cells. The DNA, which was extracted from the sperm of salmon fish, is soluble in water-methanol solution[28]. DNA solutions of different weight percentages were prepared using 9 ml of anhydrous methanol and 1 ml of deionized water. All the chemicals used were purchased from Sigma Aldrich.

First, DNA fibres were dissolved in deionized water and the solution was stirred until total transparency. Then anhydrous methanol was added to the mixture to achieve the required concentration. The solution was stirred overnight and filtered using the sterile disposable PVDF 0.22-μm vacuum filter unit. These solutions were spin-coated on silicon substrates at 5000 rpm for 30 s to produce films, which were kept overnight in a glove box with nitrogen atmosphere. All the substrates used were non-textured, one-side polished (FZ) *n*-type c-silicon (100) wafers with a thickness of 280 μm and resistivity of 2 Ω cm. A self-built ellipsometer with a deuterium halogen lamp as the light source and spectral range from 240 nm to 1150 nm was used to characterize the DNA films[29]. For the transfer-length method (TLM) measurement, 300-nm aluminum (Al) was thermally evaporated on these films using a shadow mask. The surface roughness of the DNA films on silicon were measured using atomic force microscopy (AFM)- (Bruker Multimode 8 with Nanoscope, Santa Barbara, CA, USA). UV-Visible-NIR spectrophotometer Lambda 950 (Perkin Elmer, Shelton, CT, USA) was employed to study the transmittance of DNA films spin-coated on transparent sapphire substrates.

X-ray and UV photoelectron spectroscopy (XPS and UPS, respectively) measurements of the films were performed with a Phoibos 150 analyzer (SPECS GmbH, Berlin, Germany) in ultra-high vacuum conditions (base pressure of 5×10^{-10} mbar). XPS measurements were carried out with a monochromatic Al K-alpha X-ray source (1486.74 eV), whereas a monochromatic He I UV source (21.2 eV) was used for UPS measurements. The energy resolution, as the FWHM of the Ag $3d_{5/2}$ peak for a sputtered silver foil, was 0.62 eV for XPS and 0.11 eV for UPS. The XPS spectra were analysed using the CASA XPS software and data were fitted for C, O, N, and P. The work function of the films was extracted from the analysis of UPS spectra.

The proof-of-concept devices were fabricated on *n*-type FZ crystalline silicon wafers. Before device fabrication, all the wafers were cleaned using 1% hydrofluoric acid in water (HF dip) for 60 s to achieve the H-terminated surface by removing the native oxide from the surface. Then, 1% of the DNA solution was spin-coated on the rear side of the wafer at 5000 rpm for 30 s and the wafers were kept in a glove box for overnight drying. Subsequently, the rear Al electrode, with a thickness of 300 nm, was thermally evaporated on the back side of the wafer. Vanadium pentoxide (V_2O_5) hole selective layer of thickness 25 nm was thermally evaporated on the front side of the wafer and the active area was defined by photolithography[15]. Following, an indium tin oxide (ITO) layer of 75 nm was deposited by sputtering that serves simultaneously as the antireflection coating and transparent electrode. Finally, after insulation of the devices by wet etching, a 2 μm thick silver grid was thermally evaporated using a shadow mask as the top contact. The Ag grid covered 4% of the active area of the solar cells. The reference device was also fabricated using the same process, but without DNA on the rear side electrode. The current density-voltage (*J*–*V*) characteristics of the solar cells were measured under standard conditions (100 mW cm^{-2}, AM1.5G spectrum) using a 94041A solar simulator (Newport, Irvine, CA, USA). Finally, the external quantum efficiency (EQE) analysis was made by using a QEX10 set-up (PV Measurements, Point Roberts, WA, USA). The schematics of the fabricated devices is shown in Figure 1.

Statistical Analysis: Measurements performed on different devices were reported as average +/- standard deviation (SD). In all cases, significance was defined as $p \leq 0.05$. Statistical analysis was conducted using GraphPad Prism software.

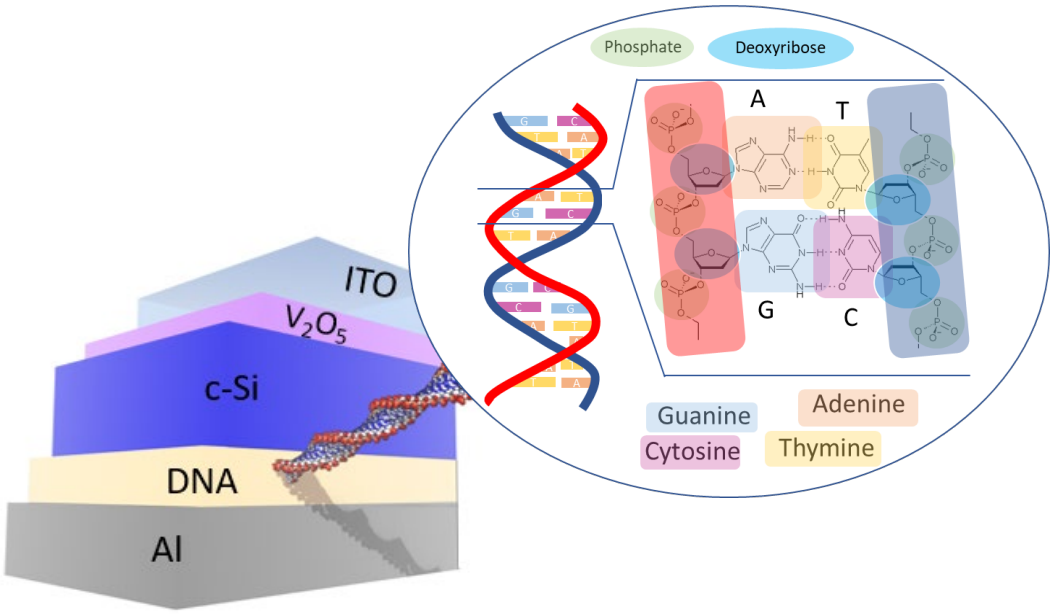

Figure 1: Schematic diagram of the fabricated devices. The inset shows the zoomed in view of double helical structure of DNA with four types of nitrogen bases: adenine (A), thymine (T), guanine (G) and cytosine (C).

Results and Discussion

DNA films used in this study were deposited on *n*-type c-Si by spin coating using solution concentrations ranging between 0.5% and 2% in 0.5% steps. The thickness of the film was 1.5 nm for the least concentrated 0.5% solution. It steadily increased to 2.5 nm for 1%, 3.3 nm for 1.5% and, finally, 5.1 nm for the highest 2% concentrated solution. The thickness vs. concentration plot follows a linear behaviour, as shown in the calibration graph included as supplementary information.

Subsequently, Al contacts were deposited on the DNA layers to characterize their electrical properties via the TLM method. The inset in Figure 2 shows the I-V characteristics of (*n*)Si/DNA/Al structures with DNA thickness between 2.5 nm and 5.1 nm. The linear I-V characteristics demonstrate a good ohmic behaviour, though the injected current rapidly decreases with the film thickness. In the TLM study the specific contact resistance can be extracted from measurements varying the contact distance. These values are shown in Figure 2 for all the DNA films. According to these results, an optimal ohmic contact is obtained for the 2.5 nm thick DNA film with a contact resistance of only 28 mΩ cm^2.

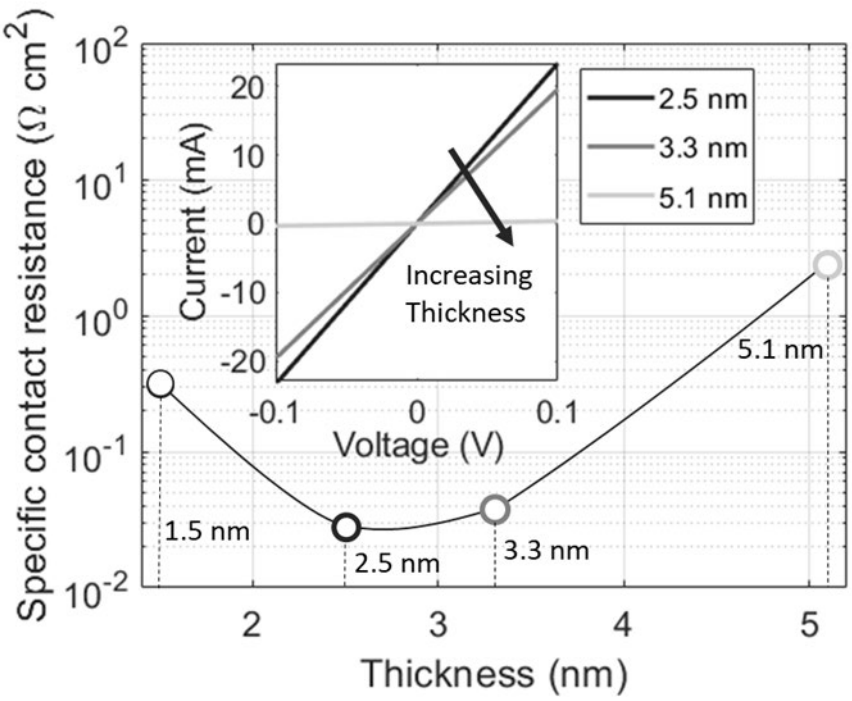

Figure 2: Specific contact resistance of Si/DNA/Al stack as a function of the DNA film thickness. The inset shows the I–V characteristics of the Si/DNA/Al stack with DNA film thickness ranging from 2.5 nm to 5.1 nm.

The presence of an optimum contact resistance at an intermediate DNA film thickness suggests that different effects need to be considered. Indeed, increased contact resistance at thicker layers is expected due to a more difficult electron transport through the organic polymer. However, the increase of contact resistance for the thinnest layer indicates that the polymer beneficial effect vanishes. Probably, Fermi level pinning at the silicon surface starts to occur as for direct metal-semiconductor contacts. This V-shaped contact resistance curve with an optimal thickness in electron tunnelling range resembles the behaviour of other selective contacts using ultra-thin intermediate dielectrics, such as magnesium oxide (MgO) or magnesium fluoride (MgF) that also operate in similar thickness ranges[30][31][14].

The topography of the DNA films was studied by AFM. The images corresponding to the samples with 2.5 nm thick and 5.1 nm thick DNA films are displayed in Figure 3. The images show rather smooth films deposited uniformly. The root mean square (RMS) roughness for the 2.5 nm thick DNA film was only 0.3 nm. The roughness does not seem to increase much with the thickness, since for the 5.1 nm thick film it was 0.4 nm. The quite similar RMS values indicate a similar structure of the films for both thicknesses. The lack of extended sharp peaks is probably associated to the amorphous structure of the film, which is preserved at different thicknesses. The results suggest an excellent wetting of the DNA solutions on the silicon surface, therefore allowing a uniform coverage over the surface.

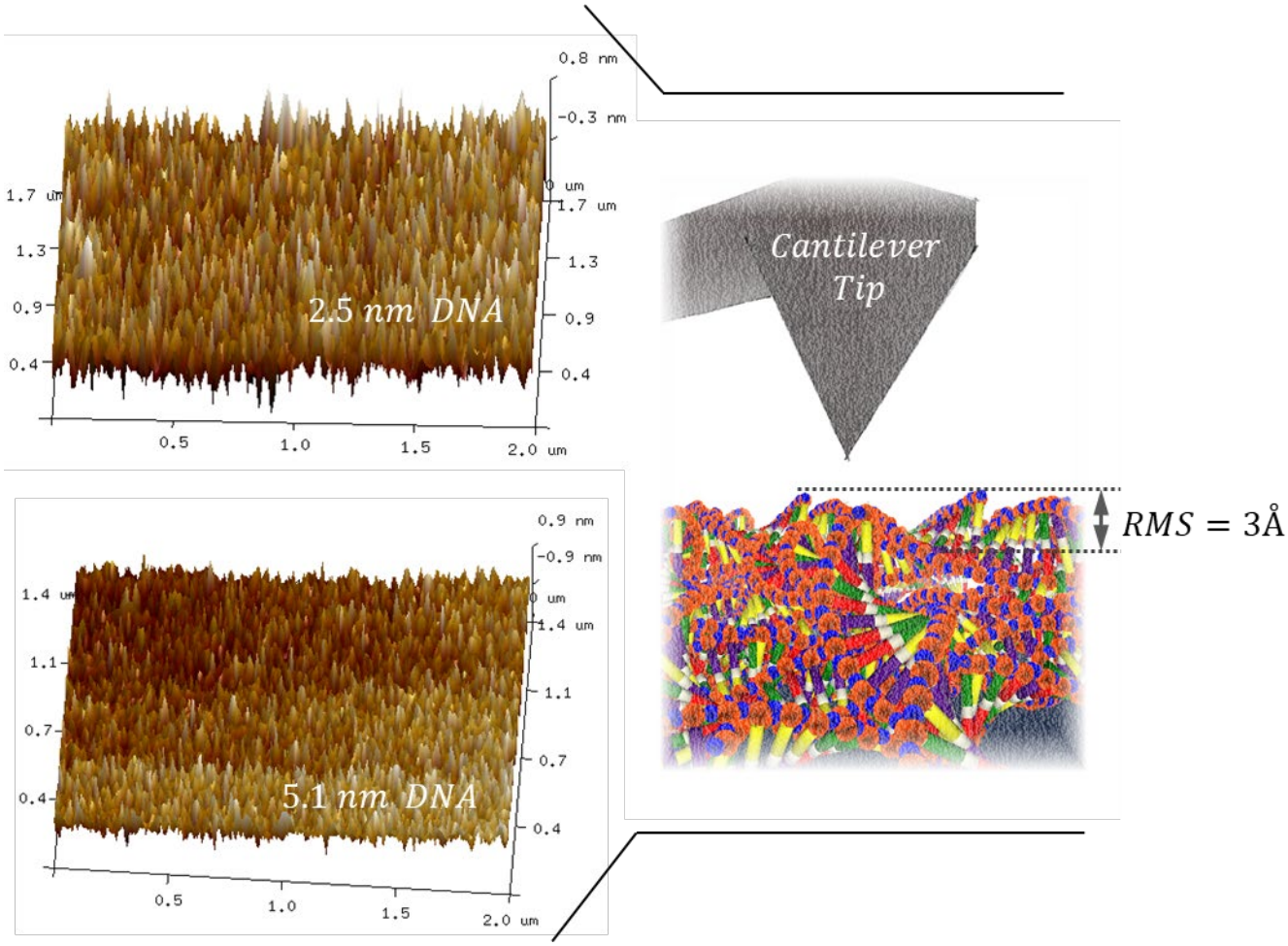

Figure 3: AFM images of DNA films with 2.5 nm and 5.1 nm thicknesses. Graphic representation of the RMS value of the surface roughness for both samples during the AFM scan.

The study of the DNA optical properties was carried out by means of UV-visible-NIR optical spectroscopy, which in turn gives information concerning the band gap energy. The transmittance spectrum within the 180–1500 nm range corresponding to the DNA films of 2.5 nm thickness (1% solution) can be seen in Figure 4. These films show almost 90% transmittance throughout the spectral regions other than in UV and visible-blue. The inset in Figure 4 shows the Tauc plot obtained from the transmittance data, with an estimated bandgap of 4.13 eV[32][33]. In this absorption plot, defined peaks at 242 nm (5.12 eV) and 266 nm (4.66 eV) are clearly seen, which have been reported throughout the literature and are generally associated to the nucleic acids and their purity [34][35]. Because of the large bandgap, the high transparency in the visible and infrared regions makes these films a suitable option also for transparent contacts.

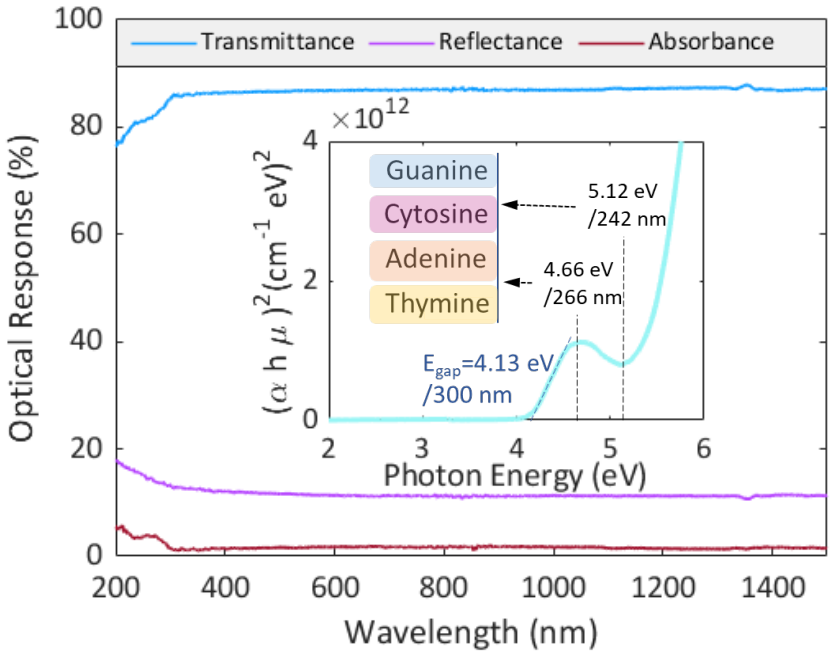

Figure 4: Transmittance, reflectance and absorbance spectra corresponding to the sample containing 2.5 nm-thick DNA 1% films. The inset shows the Tauc plot for the same sample, where the band gap energy is written down.

Chemical analysis through XPS allowed for the characterization of the four principal elements (C 1s, O 1s, N 1s, P 2p; H is not observable by XPS) of DNA, whose spectra corresponding to the thickest sample are presented in Figure 5. The main C 1s spectrum shows the characteristics of different nucleobases present in the DNA molecule; peaks at 288.9, 287.9, 286.5, and 284.9 eV correspond to urea, amide, carbon bond to nitrogen, and hydrocarbons, respectively, which represent the main electronic configurations along the double stranded structure. The largest peak of the O 1s at 532.5 eV corresponds to the oxygen bond to a phosphate group, whereas peaks at 533.1 and 531.1 eV are ascribed to C=O and metal carbonate peaks, respectively. In high concentration of DNA films (5.1 nm) the phosphate peak is highly appreciated and the P 2p peak of the phosphate group has been deconvoluted into two subpeaks with the main $2p_{3/2}$ component at 133.7 eV and $2p_{1/2}$ at 133.0 eV, with a splitting value of 0.7 eV. Phosphorus signal indicates the presence of the phosphate groups along the polymer. The principal nitrogen N 1s signal has been deconvoluted into two major peaks: one at 399.0 eV, which represents the contribution of N atoms in the double bonds with C (N=C), and another at 400.3 eV, attributed to the N singly binding with C and H, and the protonated N peaks. Such positively charged N atoms lead to charge transfer across the interlayers that could explain dipole formation in DNA films[36][37][38].

UPS analysis was also done to get a further understanding on the electronic properties of the DNA films on silicon (Figure 6). Particularly, the work function (*WF*) that is the energy required to extract an electron from the material to the vacuum level (i.e., null potential energy) can be calculated. Whereas the *WF* of the reference *n*-type silicon is 4.28 eV, in good agreement with the expected value[39], a thin DNA film reduces the calculated *WF* down to 3.28 eV. This suggests that DNA is playing a relevant role to tune the apparent interface work function allowing for a specific charge carrier to be injected or extracted. These interface properties of thin DNA films can be used to explain the low specific contact resistance of the films on silicon

obtained by TLM (Figure 3). The DNA films would depin the Fermi level from the Si surface to enhance, in our case, electron injection and extraction from the semiconductor. This property could be used in semiconductor devices as an interface modifier to promote the charge-carrier selectivity at the electrodes. As a preliminary conclusion, DNA films exhibit good potential to be used as an ETL selective contact for silicon heterojunction devices.

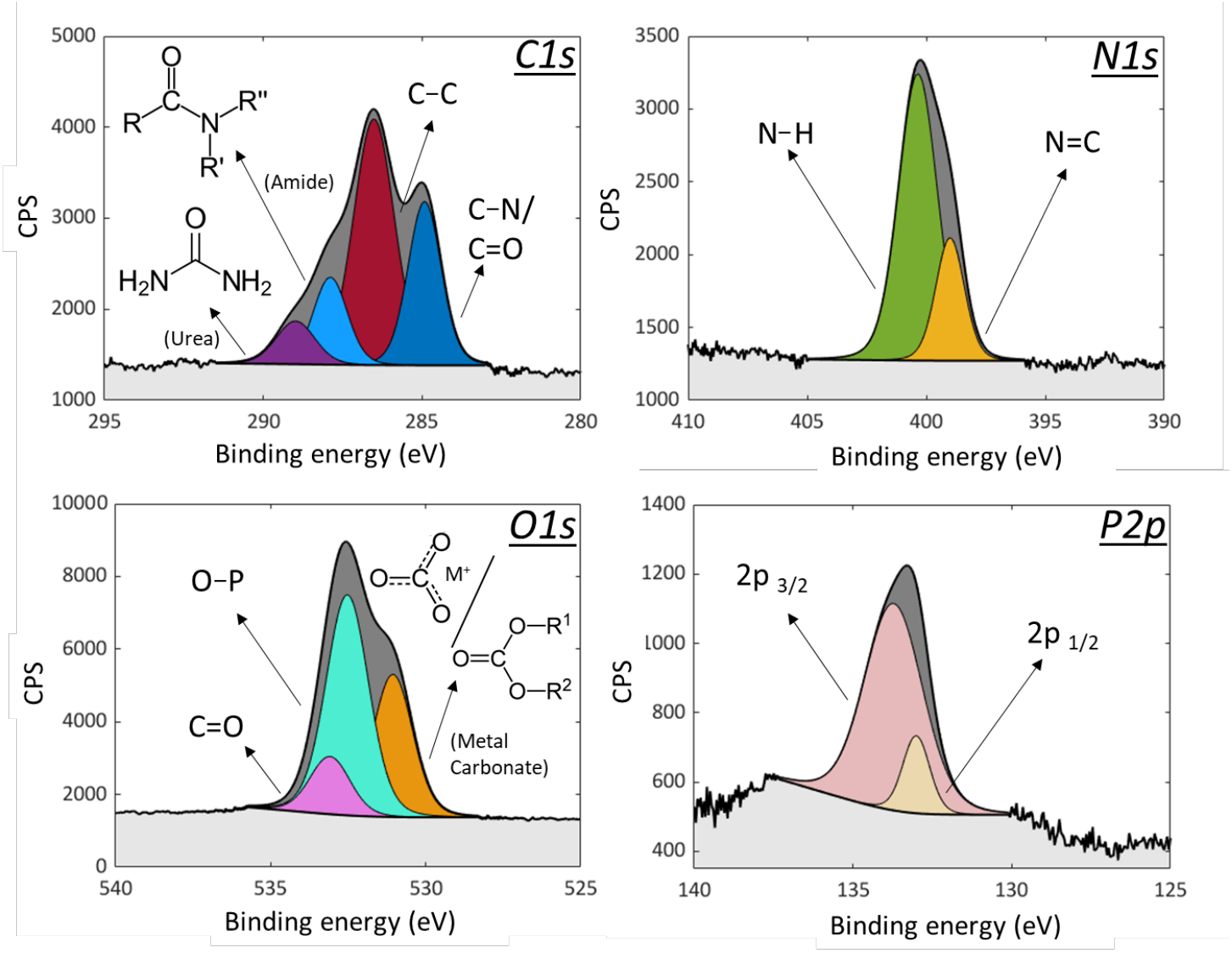

Figure 5: High-resolution XPS spectra corresponding to the four main observable elements in 5.1 nm DNA films.

On the other hand, UPS allows determining the valence band edge of the material from the cut-off of the lowest binding energy, which represents the difference between the Fermi level and the maximum of the valence band. The valence band energy edge obtained for both silicon reference and DNA films on silicon are represented in Figure 6b, after correcting the spectral region displayed in the inset of Figure 6a for the system excitation energy. One can see that the valence band edge of the reference sample is about 1 eV below the Fermi level, as expected for *n*-type silicon. On the other hand, the valence band edge is about 3.2 eV below the Fermi level for the DNA film. Considering an optical gap of 4.1 eV with the valence band

edge at 3.2 eV, we can deduce some sort of *n*-type character for the DNA films[40][41]. Such *n*-type behaviour of the DNA films may be beneficial in the heterojunction for electron extraction. However, since the conduction band edge (lowest unoccupied molecular orbital – LUMO) of the film is still about 0.9 eV higher than the silicon conduction band edge, we do not expect any significant charge transport via thermionic emission at room temperature. Instead, electron extraction could take place via either hopping within the layer or other conduction mechanisms, such as direct or trap-assisted tunnelling.

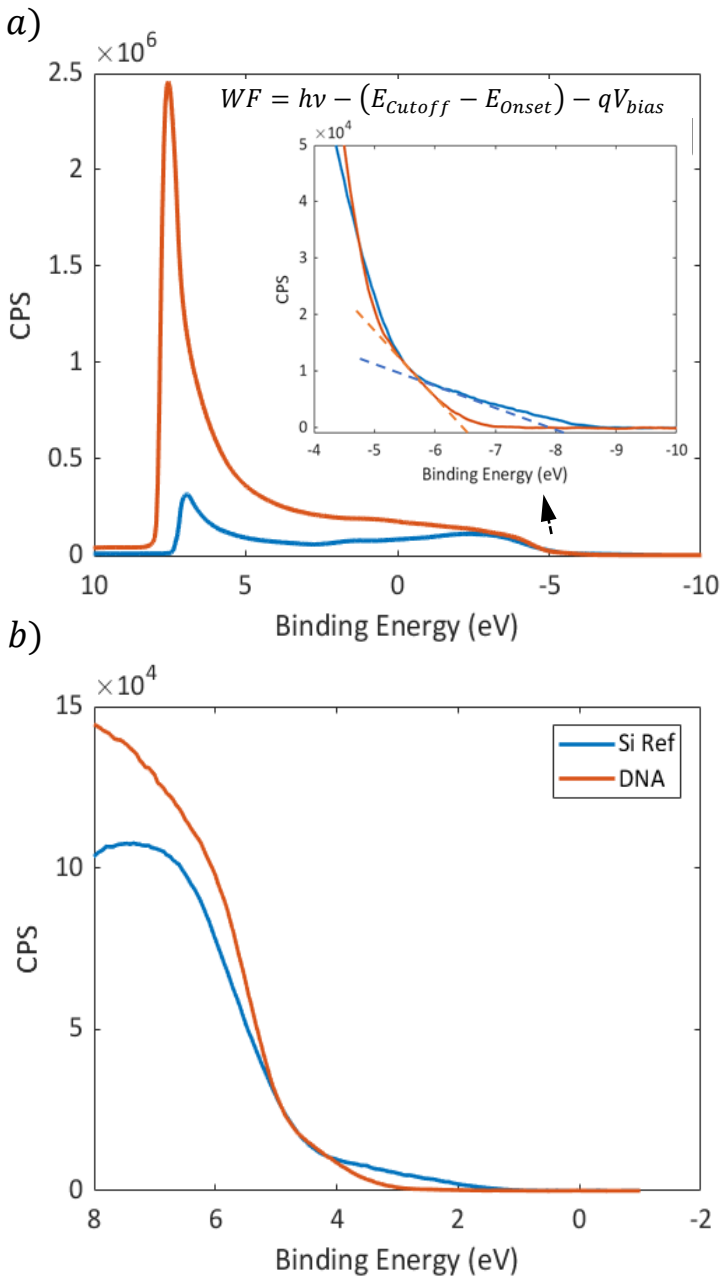

Figure 6: Analysis on the UPS spectra carried out to determine (a) the work function and (b) the valence band corresponding to silicon (in blue) and 2.5 nm DNA films (in orange). The inset in (a) shows the (non-corrected) cut-off of the lowest binding energy region, displayed in (b) after system-correcting.

In order to visualize these results, we can propose a band diagram on the basis of the work function values and valence band edges estimated from UPS measurements (see Figure 7). This energy band diagram, displayed in Figure 7, can be used to suggest a possible explanation to the good electron transport of c-Si/DNA/Al heterojunctions. The DNA film would behave as a thin dipolar interlayer, whose origin might be related to the phosphate and amino groups registered in the deconvolution of XPS spectra. The dipole formation between the semiconductor and an external electrode results in a vacuum level shift with an apparent reduction of the metal work function. As a consequence, an important charge transfer from the Al electrode to Si is expected. This effect would counteract Fermi level pinning and result in a region with majority carrier accumulation[27][30]. This electron doping of the Si surface is in good agreement with the reduction of specific contact resistance observed in TLM measurements (see Figure 2). On the other hand, the optical electron extraction through the LUMO level of the DNA film is not possible as there is a roughly 0.7 eV barrier. The most plausible conduction mechanisms through the junction must be either direct or trap-assisted tunnelling. This agrees with the need of an extremely thin layer to have a low contact resistance, as seen in the TLM measurements.

Finally, a photovoltaic device was fabricated to evaluate the performance of DNA implemented as an ETL at the corresponding electrode. The complete heterojunction solar cell structure was ITO/V_2O_5/c-Si/DNA/Al with an active area of 1×1 cm^2. A schematic diagram of this dopant-free device architecture was already anticipated in Figure 1. The solar cell was fabricated on a flat c-Si wafer, thus there is room to increase the current density up to 4 mA cm^{-2} when using texturized substrates. Thermally evaporated V_2O_5 was used as the HTL and neither passivating layers nor doped a-Si:H layers were used in the whole heterojunction device. On top of the HTL, an ITO layer was sputtered as the front transparent electrode with a sheet resistance of 120 Ω_{sq}. The top contact was finished with a 1.5 μm thick metallic grid of silver. As the rear contact, optimized DNA films of 2.5 nm (1% solution) where spin-coated on top of HF-cleaned silicon and covered with an evaporated Al layer of 500 nm. Figure 8 compares the electrical characteristics under AM1.5 illumination of Si heterojunction solar cells with and without the rear DNA layer. The corresponding photovoltaic parameters of these solar cells are summarized in Table 1. The solar cell implementing the DNA-based ETL exhibited a remarkable increase in the fill factor (*FF*) of over 12% with respect to the reference device without such interlayer. The high *FF* value up to 76.7% could be linked to the elimination of Fermi level pinning as well as a reduced contact resistance by electron accumulation. Moreover, the open circuit voltage (V_{oc}) is also substantially increased from 339.8 mV to 600.0 mV. The low V_{oc} value of the reference solar cell suggests the presence of an interface energy barrier. Consequently, part of the internal quasi-Fermi level separation would be lost at the rear electrode for electron extraction. Finally, an increase of about 5 mA cm^{-2} in the short circuit current density (J_{sc}) has been also observed, probably related to the surface passivation provided by effect of the DNA layer. As a result of all the exposed arguments, the power conversion efficiency of the DNA-based solar cell exceeded 15%, thus more than double that of the reference device. In summary, the results hereby reported reveal that the efficiency and overall performance of Si heterojunction-based solar cells can be improved by introducing a dipolar layer based on DNA films between the semiconductor and the metal electrode, which promotes photogenerated carrier extraction. As well, processing of such additional interfacial layer does not affect the fabrication process in terms of time, thermal budget or cost, given that the DNA films deposition is done via a fast and non-toxic technique.

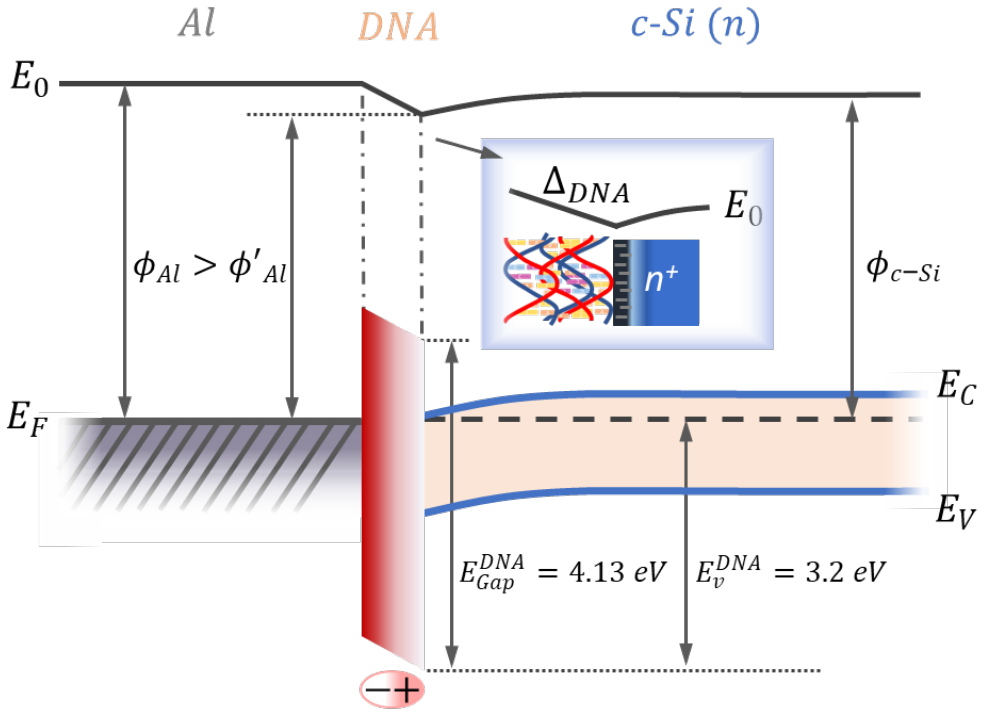

Figure 7: Energy band diagram corresponding to the Si/DNA/Al heterojunction under study.

Table 1. PV parameters corresponding to the DNA film-based and the reference cells.

Rear contact	***c-Si/Al***	***c-Si/DNA/Al (mean ± SD)***	***c-Si/DNA/Al (best cell)***
FF (%)	*64.4*	*75.1 ± 0.7*	*76.8*
V_{oc} (mV)	*340*	*601 ± 2*	*600*
J_{sc} (mA cm^{-2})	*28.3*	*32.5 ± 1.5*	*33.8*
PCE (%)	*6.2*	*14.5 ± 0.8*	*15.6*

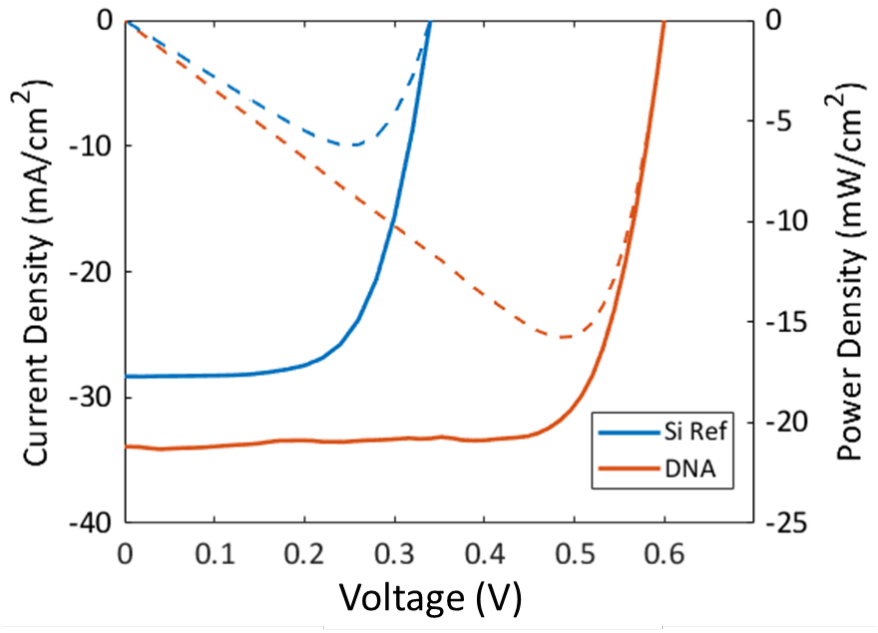

Figure 8: J–V (solid lines) and P–V (dashed lines) curves from the DNA film-based (orange) and the reference (blue) cells.

Conclusion

This work reports the deposition and characterization of thin DNA films deposited by spin coating of methanol solutions, and their use in a metal/semiconductor junction as a buffer layer to provide enhanced electron injection/extraction (ETL). AFM images confirmed deposition of smooth and rather uniform films (0.3–0.4 nm roughness). Tauc plots obtained from optical transmittance from the DNA films show the presence of nucleic bases through the peaks at 4.66 eV and 5.12 eV, and an optical gap of 4.13 eV has been determined. XPS analysis further proved the presence of all expected organic compounds of DNA in the deposited thin films. Soft XPS analysis of DNA allowed locating the valence band (highest occupied molecular orbital –HOMO– level) 3.2 eV below the Fermi level, which suggests a possible *n*-type doping of the film. Specific contact resistance values extracted from TLM measurements evidence a clear reduction for a DNA thin layer around 2 nm. Finally, UPS spectra confirmed a work function shift with respect to the reference silicon sample of roughly 1 eV.

This reduction of the electrode work function might be the main working principle of the DNA films, as it promotes electron migration from the metal into the silicon. In turn, this causes an unintentional doping by electron accumulation similar to the case of using low-work function metals such as magnesium or calcium. We have provided a schematic representation of the expected situation in terms of the energy band structure at the junction. Due to the fact that the LUMO level of the DNA film is 0.7 eV above the conduction band of the silicon, the operation of DNA films as selective contacts in a traditional way, i.e., through thermionic emission of electrons from silicon, seems not plausible. Instead, the strong dependence with

the DNA film thickness suggests that electrons are directly tunnelled into the electrode, in agreement with the optimum thickness obtained from TLM experiments.
Finally, in order to prove the potential of these films in a complete device, a solar cell test structure has been fabricated using completely dopant-free selective contacts in a non-textured wafer. The resulting proof-of-concept solar cell achieved an efficiency higher than 15.6%, with a remarkable improvement in all the photovoltaic parameters. This effect could be attributed to the elimination of Fermi level pinning, as well as to a better surface passivation and charge-carrier extraction due to electron accumulation at the silicon surface. In conclusion, a significant improvement of electron transport in solar cells fabricated with a DNA buffer has been confirmed. Furthermore, the possibilities of using thin DNA films for enhanced electron transport in different electronic devices go far beyond the photovoltaic applications and should be considered as an interesting technology route.

Acknowledgements

This research has been supported by Spanish government through grants PID2019-109215RB-C41, PID2019-109215RB-C43, and PID2020-116719RB-C41 funded by MCIN/AEI/10.13039/501100011033. One of the authors (T. Tom) acknowledges the support of the Secretaria d'Universitats i Recerca de la Generalitat de Catalunya and European Social Fund (2019 FI_B 00456). Besides this, the authors thank technical staff from Barcelona Research Center in Multiscale Science and Engineering from Universitat Politècnica de Catalunya for its expertise and helpful discussions over XPS results, Dr. Oriol Arteaga Barriel from Universitat de Barcelona for the thickness measurements and also Guillaume Sauthier from Catalan Institute of Nanoscience and Nanotechnology for his contribution through UPS measurements and discussions.

References:

[1] R. G. Endres, D. L. Cox, R. R. P. Singh, *Rev. Mod. Phys.* **2004**, *76*, 195.
[2] G. J. V. Nossal, *Nature* **2003**, *421*, 440.
[3] F. H. Watson, J. D.; Crick, *Nature* **1953**, *171*, 737.
[4] E. M. Heckman, J. A. Hagen, P. P. Yaney, J. G. Grote, F. K. Hopkins, *Appl. Phys. Lett.* **2005**, *87*, 1.
[5] L. Wang, J. Yoshida, N. Ogata, S. Sasaki, T. Kajiyama, *Chem. Mater.* **2001**, *13*, 1273.
[6] A. J. Steckl, *Nat. Photonics* **2007**, *1*, 3.
[7] J. A. Hagen, W. Li, A. J. Steckl, J. G. Grote, *Appl. Phys. Lett.* **2006**, *88*, 3.
[8] Y. Zhang, P. Zalar, C. Kim, S. Collins, G. C. Bazan, T. Q. Nguyen, *Adv. Mater.* **2012**, *24*, 4255.
[9] L. Wan, C. Zhang, K. Ge, X. Yang, F. Li, W. Yan, Z. Xu, L. Yang, Y. Xu, D. Song, J. Chen, *Adv. Energy Mater.* **2020**, *10*, 1.
[10] T. G. Allen, J. Bullock, X. Yang, A. Javey, S. De Wolf, *Nat. Energy* **2019**, *4*, 914.
[11] T. Zhang, S. Iqbal, X. Y. Zhang, W. Wu, D. Su, H. L. Zhou, *Sol. Energy Mater. Sol. Cells* **2020**, *204*, 0.
[12] J. Yu, J. Yu, J. Yu, P. Phang, C. Samundsett, R. Basnet, G. P. Neupan, X. Yang, D. H. Macdonald, Y. Wan, D. Yan, J. Ye, *ACS Appl. Mater. Interfaces* **2020**, *12*, 26177.

[13] J. Bullock, P. Zheng, Q. Jeangros, M. Tosun, M. Hettick, C. M. Sutter-Fella, Y. Wan, T. Allen, D. Yan, D. Macdonald, S. De Wolf, A. Hessler-Wyser, A. Cuevas, A. Javey, *Adv. Energy Mater.* **2016**, *6*, 1.
[14] Y. Wan, C. Samundsett, J. Bullock, T. Allen, M. Hettick, D. Yan, P. Zheng, X. Zhang, J. Cui, J. McKeon, A. Javey, A. Cuevas, *ACS Appl. Mater. Interfaces* **2016**, *8*, 14671.
[15] T. Tom, E. Ros, N. López-Pintó, J. Miguel Asensi, J. Andreu, J. Bertomeu, J. Puigdollers, C. Voz, *Materials (Basel).* **2020**, *13*, 4905.
[16] H. T. Nguyen, E. Ros, T. Tom, J. Bertomeu, J. M. Asensi, J. Andreu, I. M. Garcia, P. Ortega, M. Garin, J. Puigdollers, C. Voz, R. Alcubilla, *IEEE J. Photovoltaics* **2019**, *9*, 72.
[17] N. Lopez-pinto, T. Tom, J. Bertomeu, J. M. Asensi, P. Ortega, C. Voz, *Appl. Surf. Sci.* **2021**, 150285.
[18] C. Battaglia, A. Cuevas, S. De Wolf, *Energy Environ. Sci.* **2016**, *9*, 1552.
[19] P. Gao, Z. Yang, J. He, J. Yu, P. Liu, J. Zhu, Z. Ge, J. Ye, *Adv. Sci.* **2018**, *5*.
[20] P. Ensslen, S. Gärtner, K. Glaser, A. Colsmann, H. A. Wagenknecht, *Angew. Chemie - Int. Ed.* **2016**, *55*, 1904.
[21] Ö. Ateş Sönmezoğlu, S. Akın, B. Terzi, S. Mutlu, S. Sönmezoğlu, *Adv. Funct. Mater.* **2016**, *26*, 8776.
[22] A. R. bin M. Yusoff, J. Kim, J. Jang, M. K. Nazeeruddin, **2016**, *9*, 1736.
[23] A. Elfwing, W. Cai, L. Ouyang, X. Liu, Y. Xia, Z. Tang, O. Inganäs, *ACS Appl. Mater. Interfaces* **2018**, *10*, 9579.
[24] Y. Hou, K. Wang, D. Yang, Y. Jiang, N. Yennawar, K. Wang, M. Sanghadasa, C. Wu, S. Priya, *ACS Energy Lett.* **2019**, *4*, 2646.
[25] J. Dagar, M. Scarselli, M. De Crescenzi, T. M. Brown, *ACS Energy Lett.* **2016**, *1*, 510.
[26] J. Dagar, G. Scavia, M. Scarselli, S. Destri, M. De Crescenzi, T. M. Brown, *Nanoscale* **2017**, *9*, 19031.
[27] C. Reichel, U. Würfel, K. Winkler, H. F. Schleiermacher, M. Kohlstädt, M. Unmüssig, C. A. Messmer, M. Hermle, S. W. Glunz, *J. Appl. Phys.* **2018**, *123*.
[28] M. A. Lever, A. Torti, P. Eickenbusch, A. B. Michaud, T. Šantl-Temkiv, B. B. Jørgensen, *Front. Microbiol.* **2015**, *6*.
[29] S. Bian, C. Cui, O. Arteaga, *Appl. Opt.* **2021**, *60*, 4964.
[30] C. Reichel, U. Würfel, J. H. Hack, K. Winkler, C. A. Messmer, H. F. Schleiermacher, M. Kohlstädt, M. Hermle, S. W. Glunz, *Sol. RRL* **2021**, *5*, 25.
[31] Y. Wan, C. Samundsett, J. Bullock, M. Hettick, T. Allen, D. Yan, J. Peng, Y. Wu, J. Cui, A. Javey, A. Cuevas, *Adv. Energy Mater.* **2017**, *7*.
[32] F. F. Maia, V. N. Freire, E. W. S. Caetano, D. L. Azevedo, F. A. M. Sales, E. L. Albuquerque, *J. Chem. Phys.* **2011**, *134*.
[33] K. Iguchi, *J. Phys. Soc. Japan* **2001**, *70*, 593.
[34] A. E. Gasperini, S. Sanchez, A. L. Doiron, M. Lyles, G. K. German, *Sci. Rep.* **2017**, *7*, 1.
[35] J. Richter, M. Nnaji, H. Park, *Polymers (Basel).* **2021**, *13*.
[36] S. Ptasińska, A. Stypczyńska, T. Nixon, N. J. Mason, D. V. Klyachko, L. Sanche, *J. Chem. Phys.* **2008**, *129*.
[37] D. Y. Petrovykh, H. Kimura-Suda, L. J. Whitman, M. J. Tarlov, *J. Am. Chem. Soc.* **2003**, *125*, 5219.
[38] W. Ji, T. Allen, X. Yang, G. Zeng, S. De Wolf, A. Javey, *ACS Energy Lett.* **2020**, *5*, 897.
[39] D. Menzel, M. Mews, B. Rech, L. Korte, *Appl. Phys. Lett.* **2018**, *112*.
[40] A. M. Shing, Y. Tolstova, N. S. Lewis, H. A. Atwater, *Appl. Phys. A Mater. Sci. Process.* **2017**, *123*, 1.

[41] M. Tsai, S. Su, J. Chang, D. Tsai, C. Chen, C. Wu, L. Li, L. Chen, J. He, M. Science, E. Engineering, M. Sciences, M. Sciences, S. Arabia, *ACS Nano* **2014**, *8*, 8317.